Remote Sensing of Environment 158 (2015) 393–406

Contents lists available at ScienceDirect

Remote Sensing of Environment

journal homepage: www.elsevier.com/locate/rse

A new perspective to assess the urban heat island through remotely sensed atmospheric profiles

Leiqiu Hu *, Nathaniel A. Brunsell

Department of Geography, University of Kansas, Lawrence, KS 66045, USA

ARTICLE INFO

Article history:
Received 10 July 2014
Received in revised form 25 October 2014
Accepted 25 October 2014
Available online 5 December 2014

Keywords:
Urban heat island
MODIS
Atmospheric profiles
Urban heat island curve
Near-surface temperature

ABSTRACT

The detection of urban heat island (UHI) is generally conducted from ground observations of air temperature and remote sensing of land surface temperature (LST). Satellite remotely sensed LST has many merits, such as global coverage and consistent periodicity, which overcomes the weaknesses of ground observations related to the footprint, site distributions, and costs. For human related studies and urban climatology, air temperatures are equally important. This study explores the potential to estimate the near-surface air and dew-point temperatures from the MODIS 07 atmospheric profile product (MOD07_L2) to capture the UHI dynamics at 5 km resolution. Four mega-cities in North America: Phoenix, Houston, Chicago, and Toronto, are evaluated during 2003–2013 summers. The comparison between the MODIS near-surface temperature and the ground observations suggests an accuracy of 3–7 K RMSE for different cities and times of day. For air temperature, the Aqua overpass has better agreements, and nighttime has higher accuracy than daytime in most cases. In general, very dry (Phoenix) and very moist (Houston) climate conditions increase the variability of the MODIS temperature accuracy. This study also develops an urban heat island curve (UHIC) to represent UHI intensity by integrating the urban surface heterogeneity in a curve, showing the relationship between air temperature and urban fraction. UHIC provides a new way to quantify UHI city by city, which emphasizes the temperature gradients, consequently decreasing the impact of data biases.

1. Introduction

Urban heat island (UHI) is a phenomenon where the urban area is warmer than its ambient rural area. The progressive modification of surface covers and structures as well as other human activities cause UHI. With a growing trend of urban populations, a threat to human health is posed due to the increased temperatures (Kalkstein & Greene, 1997; Patz, Campbell-Lendrum, Holloway, & Foley, 2005) and air pollution (Mage et al., 1996; Taha, 1997) in urban environments, which has created wide public concern, especially under global climate changes. To solve these problems requires intensive investigations of UHI at multiple scales.

UHI studies are well documented across time and space by using various measuring techniques and temperatures as summarized by Voogt and Oke (2003). Two distinct classes of UHI are often defined: atmospheric UHI is assessed through in-situ and vehicle mounted sensors measuring air temperatures in the urban canopy layer (UCL) (Oke, 1976) and through ground-based, airborne and tower mounted sensors for the urban boundary layer (UBL) (Barlow et al., 2011; Grimmond, 2006; Roth, 2000; Voogt & Oke, 2003); the second class is surface UHI (SUHI) and is based on the use of thermal remotely sensed data (Voogt & Oke, 2003). Traditionally, the atmospheric UHI magnitude is defined/estimated by comparing air temperature in urban and rural sites (Grimmond, 2006). However, measurements for atmospheric UHI at urban sites face substantial challenges. Oke (2008) addressed the detailed siting and exposure requirements for measurements. Stewart (2011) pointed out that about a half of 190 observational UHI studies have not sufficiently controlled for the essential effects of weather, relief or time to quantify UHI intensity. Moreover, the limited footprint of a ground-based measurement makes it difficult to capture a comprehensive distribution of temperature over highly heterogeneous urban areas. To solve these problems, usually a well-designed network of stations is required. Perhaps, an easy and straightforward approach would be to use a consistent gridded dataset of observations, such as those from satellite remote sensing.

SUHI research is thriving after land surface temperature (LST) data became available (Gallo, Tarpley, Mcnab, & Karl, 1995; Voogt & Oke, 2003). Moreover, the global coverage, temporally consistent LSTs from satellite observations provide a way to estimate air temperature distributions, but the relationship of LST and air temperature remains empirical (Voogt & Oke, 2003). To link the LST and air temperature, many factors must be considered, such as the surface properties, atmospheric conditions and solar angles (Kim & Han, 2013; Vancutsem, Ceccato, Dinku, & Connor, 2010). Therefore, it becomes difficult to get a simple and consistent estimation for a large area. The air temperature directly retrieved from satellite remote sensing probably has more potential for universal

* Corresponding author at: National Center for Atmospheric Research, P.O. Box 3000, Boulder, Co 80307.
E-mail address: leiqiu@ucar.edu (L. Hu).

http://dx.doi.org/10.1016/j.rse.2014.10.022
0034-4257/

applications of UHI and human health related research, which avoids the scaling issues and the problems associated with the different essential physical factors impacting those two types of temperatures.

The atmospheric temperature and moisture profiles are important descriptors of the urban environment. Kidd, Levizzani, and Bauer (2009) summarized the progress of satellite-based atmospheric observations and discussed the applications of retrieved atmospheric parameters for improving weather forecasting, extending weather systems' monitoring ability, and understanding climate change. Sounding sensors are typically designed with horizontal resolutions from tens to hundreds of kilometers. For application over the urban area, the coarse spatial resolutions may fail to capture the surface heterogeneity over the urban area.

Temperature and moisture information retrieved from MODIS at 5 km horizontal resolution can bridge gaps in an atmospheric UHI study that requires observations with relatively high spatial and temporal resolution. These global-coverage data are not only used for atmospheric effect corrections of other MODIS products, such as sea/land surface temperature (SST/LST), but also for capturing the atmospheric features of column water vapor and ozone (Seemann, Borbas, Li, Menzel, & Gumley, 2006; Borbas et al., 2011). However, the applications of MODIS atmospheric profiles are only discussed in a few studies outside the MODIS product groups, such as the MODIS-based estimation of net radiation (Bisht & Bras, 2010; Bisht, Venturini, Islam, & Jiang, 2005; Wang & Liang, 2009) and potential evapotranspiration (Kim & Hogue, 2008). These studies directly estimated the surface temperature and moisture from MODIS profiles without quantifying the accuracy. The error propagation from the MODIS product may explain part of the errors in their estimations.

Moreover, the spatial distribution of temperature does not solve UHI quantification problems as a result of unclear urban–rural division at the current stage (Stewart, 2011). Schwarz, Lautenbach, and Seppelt (2011) concluded that different SUHI indicators have weak correlations, and emphasized the critical role of choosing indicators to quantify SUHI effects. It becomes very difficult to conduct an intercomparison among the UHI studies in the literature due to the unstandardized indicators. Consequently, a better way to quantify UHI magnitude is required considering the surface heterogeneity and ambiguous urban/rural boundaries.

The purpose of this study is to provide an innovative analysis for using MODIS retrieved near-surface air temperature to investigate the UHI. This study first assessed the accuracy of the near-surface air and dew-point temperatures from MODIS 07 atmosphere profiles over four mega-cities in North America by using long-term ground observations. Both day and night overpasses of Terra and Aqua were investigated due to the potential applications to address diurnal UHI effects. Moreover, according to the strengths of MODIS air temperature, we developed a city-dependent UHI curve as a function of urban fraction, which is able to integrate the spatially heterogeneous physical properties and long-term variations of temperature to quantify UHI intensity.

2. Study area and data

2.1. Study area

Four mega cities in North America are selected for this research: Phoenix, Houston, Chicago and Toronto. Fig. 1 shows the domains and 2012 land cover distributions of the four cities. According to NOAA's national coastal population report, about 39% of the U.S. population lived in coastal areas in 2010 (NOAA National Ocean Service, 2013), so three cities located near/on the shoreline were chosen. Chicago and Toronto, with similar geographic location and prevailing weather conditions, are featured as the humid continental climate with warm/hot and humid summers. Although, the higher latitude and location near the Great Lakes may help decrease the energy consumption for air conditioning, the population growth and climate change may put these cities under the exposure of a higher heat vulnerability. Houston is located in the humid subtropical climate zone, known for hot and very humid summers. Phoenix is under a subtropical desert climate with extremely hot and clear summers. It is important to include cities with very clear and very cloudy summers to extend the understanding of the performance of the MODIS data.

2.2. Satellite data

The MODIS atmospheric profile product (MOD07_L2 for Terra and MYD07_L2 for Aqua, hereafter MOD07_L2 for MODIS 07 product) for 5-minute Level-2 Collection-6 was processed from 2003 to 2013 in June–July–August (JJA) for both daytime and nighttime overpasses. The median local standard time of each satellite overpass for four cities ranges from 10:30–11:05 (Terra-Day), 21:15–22:15 (Terra-Night), 12:25–13:20 (Aqua-Day), and 1:35–2:10 (Aqua-Night). MOD07_L2 product consists of temperature and moisture profiles (20 pressure levels: 5, 10, 20, 30, 50, 70, 100, 150, 200, 250, 300, 400, 500, 620, 700, 780, 850, 920, 950, and 1000 hPa), total-ozone burden, atmospheric water vapor and other atmospheric information under clear skies at 5 km horizontal resolution.

The MOD07_L2 temperature and moisture sounding data are retrieved from MODIS multispectral thermal radiation measurements. The MODIS retrieval algorithms (Seemann et al., 2006) are adjusted from the TIROS (Television Infrared Observation Satellite) Operational Vertical Sounder (TOVS) algorithms (Reale, 2002) and Geostationary Operational Environmental Satellite (GOES) Atmospheric Sounder algorithms (Menzel & Purdom, 1996), which are based on a statistical regression retrieval (Seemann, Li, Menzel, & Gumley, 2003). Further details regarding the retrieval algorithm and MOD07_L2 Collection 6 quality can be found in the product algorithm theoretical basis document (Borbas et al., 2011). In general, MODIS has a limited ability to capture the fine-scale vertical structure compared to the high spectral resolution sounding sensors (e.g. Atmospheric Infrared Sounder (AIRS) (Aumann et al., 2003)), but it provides higher horizontal resolution of temperature and moisture distributions. This is useful to help understand the urban climate by capturing the urban surface heterogeneity globally for a long-term perspective.

However, the MODIS atmosphere product could not avoid some issues which is related to the nature of remote sensing techniques. For example, the view angle impacts the land surface temperature in the MODIS products (Hu, Brunsell, Monaghan, Barlage, & Wilhelmi, 2014) even when the retrieval algorithm considers the view angle influences. Moreover, thermal anisotropy widely exists in the urban surface. These issues will not be addressed in this study, but need to be considered for studies where higher accuracy is required.

To estimate the near-surface air temperature, the digital elevation model (DEM) from U.S. Geological Survey (USGS)'s National Elevation Dataset (NED) was used instead of the surface elevation (SE) layer from the MOD07_L2 product. The SE varies temporally, which is estimated from the surface pressure. To match the spatial resolution of the MOD07_L2 product, the DEM is upscaled from the original 30 m to 5 km by averaging. The mean differences between DEM and SE over the area with less terrain variations (where most of the cities are located) are small, while the mountainous areas result in larger gaps up to 100–200 m.

The yearly MODIS land cover product (MCD12Q1) at 500 m resolution from 2003 to 2012 was used for discrimination of urban and rural pixels in UHI analysis. The 2012 land cover information was used for 2013 due to the unavailability of 2013 land cover data.

2.3. Ground observations

The Integrated Surface Global Hourly observations from the National Climatic Data Center (NCDC) (http://www.ncdc.noaa.gov/cdo-web/datasets) were used for validation. Ground observations were filtered based on the following criteria: 1) observational data passed all the quality control checks, 2) the ground observation time was within ± 1 h of satellite overpass, and 3) the observation sites were within

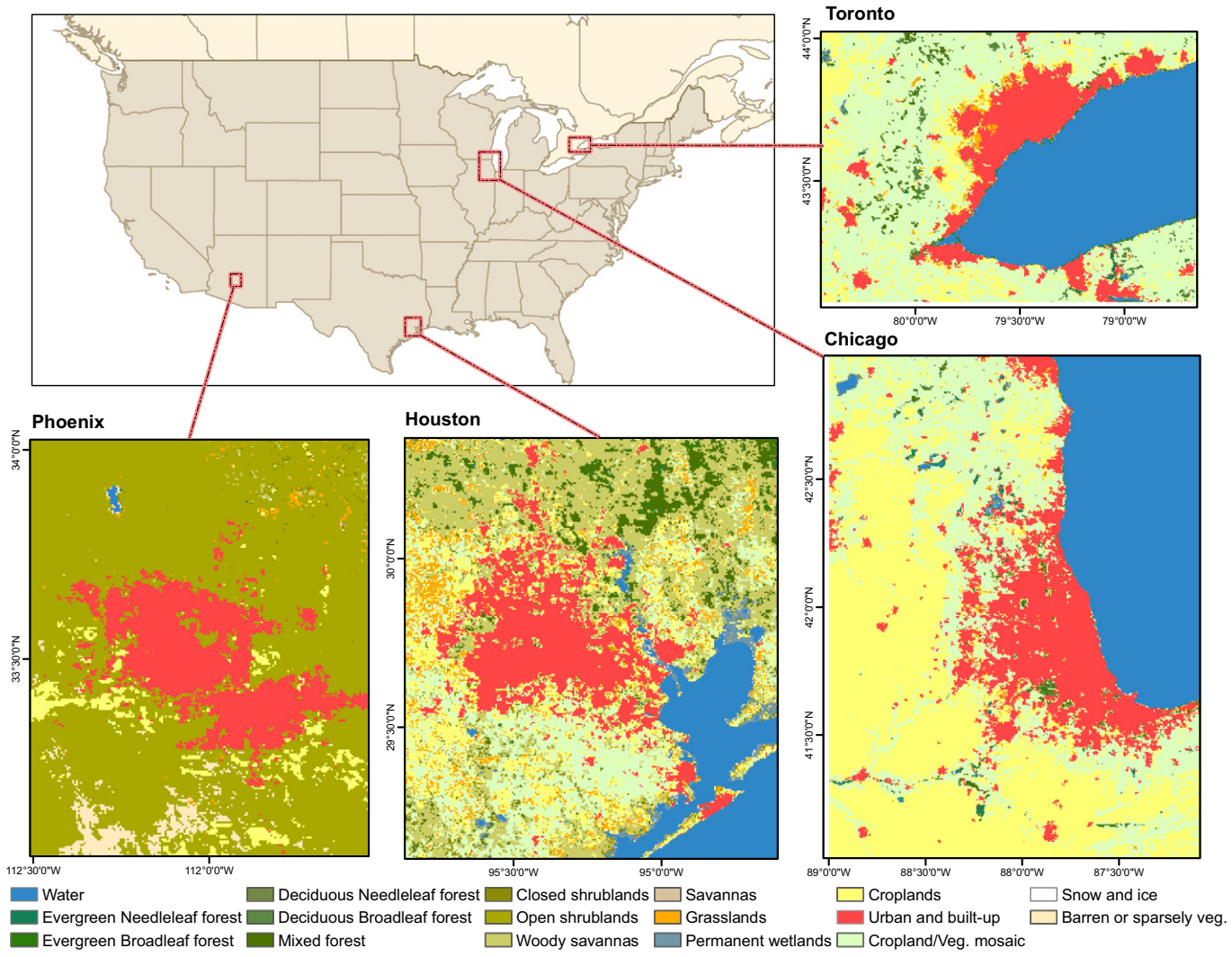

Fig. 1. The city domains and the land cover distributions in 2012 of four cities: Phoenix, Houston, Chicago, and Toronto. The land cover maps are IGBP land cover classification from MODIS MCD12Q1 product at 500 m.

the study domains. After preliminary statistics, the site in Elora RCS, Toronto (USAF ID: 713520) was removed due to the presence of many below-freezing records in summer. Fig. 3 illustrates the ground observation locations with a black unfilled circle (sites in the 5 km pixel not classified as a water pixel) and a black cross (sites in the 5 km pixel with water pixels). A summary of the ground sites is given in Table S1 in the supplemental document. (Hereafter, the table and figures with the prefix 'S' can be found in the supplemental document.)

3. Methodology

The MOD07_L2 is formatted in an orbital swath. The primary reprocessing requires mosaicing, reprojection and subsetting, which were done by using HDF-EOS to GeoTIFF Conversion Tool (HEG) (http://newsroom.gsfc.nasa.gov/sdptoolkit/HEG/HEGHome.html). The layers from MOD07_L2 air temperature, dew-point temperature, and geopotential height profiles (converted to geometric height), and the DEM from USGS were converted into a consistent extent and resolution for each city.

3.1. Instantaneous near-surface air and dew-point temperatures

The MODIS atmospheric profiles are retrieved based on multiple shortwave and longwave infrared bands by a statistical regression algorithm, which uses the coefficients from a radiative transfer model and atmospheric features from a global radiosonde dataset (Seemann et al., 2003). The methodology to estimate the near-surface air and dew-point temperature (T_a^S and T_d^S) was to extrapolate the lowest pressure level temperature/moisture information (T_a^L and T_d^L) from MOD07_L2 profiles to the surface elevation from the DEM under the hydrostatic atmosphere assumption. For the cities considered here, the typical lowest pressure levels derived over the urban areas are 920 hPa for Phoenix, 1000 hPa for Houston, and 950 hPa for Chicago and Toronto. Because the estimation is primarily determined by the mean surface elevation at 5 km resolution, it does not explicitly distinguish between urban and rural surface structures. Although we called this the “near-surface” temperature, it is more likely to be at the base height within the UBL over cities and their surroundings.

First, the geopotential height is converted to geometric height based on the gravity of the city locations. Bisht and Bras (2010) use a constant lapse rate (6.5 K/km) over the Southern Great Plains. However, considering the urban surface heterogeneity, environment lapse rate (Γ_e) was assumed to vary spatially and was calculated for each pixel by using temperature and height information at the two lowest layers of the profiles:

$$\Gamma_e = -\frac{\partial T}{\partial z} \simeq -\frac{T_a^{L1} - T_a^{L2}}{z^{L1} - z^{L2}} \quad (1)$$

where T_a^{L1} and T_a^{L2} are the air temperature at the lowest and the second lowest levels of MODIS sounding near the surface; and z^{L1} and z^{L2} are the geometric heights corresponding to T_a^{L1} and T_a^{L2}.

Assuming that the lapse rate is constant near the surface for each pixel, Γ_e at the lowest profile level was applied to the surface level. The near-surface air temperature (T_a^S) can be calculated by:

$$T_a^S = T_a^{L1} - \Gamma_e\left(z^S - z^{L1}\right) \quad (2)$$

where z^S is surface elevation from the DEM. The elevation differences ($z^S - z^{L1}$) are approximately less than 50 m over the four urban areas.

Due to these small elevation differences, Eqs. (1) and (2) can be applied to estimate the near-surface dew-point temperature (T_d^S) through the use of a dew-point lapse rate (Γ_w) and the dew-point temperatures at the two lowest levels (T_d^{L1} and T_d^{L2}) of MODIS profiles.

The MOD07_L2 product quality is sensitive to the presence of clouds and cloud contamination detection. The MODIS cloud mask product (MOD35_L2) was used for cloud screening. Moreover, the profile retrieval requires at least 5 out of 25 pixels (1 km resolution at nadir) in a 5 × 5 field-of-view area (around 5 km) with a 95% or greater confidence of clear sky (Borbas et al., 2011). In addition to clouds, other factors may cause unrealistic profiles, e.g. a sharp change in atmospheric structure. Quality controls were applied to the near-surface air and dew-point temperatures to exclude unrealistic atmospheric profiles and near-surface temperatures. We removed a few outliers that the MODIS air temperatures are higher or lower than the historic monthly records in the summers ±5 K. For example, the high threshold for Phoenix is 328 K (323 + 5 K), while the low threshold is 277 K (282 − 5 K). The 5 K buffer was set for the possible bias for MOD07_L2 product. Also, the pixels with a dew-point temperature higher than the air temperature were considered invalid pixels under clear sky conditions.

Fig. 2 shows an example of mean temperature and moisture profiles for the lower nine pressure levels with retrieved near-surface temperature and ground observations. The profile is averaged from one urban pixel, with a ground station under most clear sky days/nights of the study area. Although, the relatively coarse vertical resolution limits the fine description of atmospheric structures, the profiles are able to capture the general state of the atmosphere under clear sky conditions.

3.2. Urban heat island curve

Current studies have investigated the relationship between UHI intensity with surface physical properties and social and economic factors, such as vegetation index (Weng, Lu, & Schubring, 2004; Weng, Rajasekar, & Hu, 2011), wind (Morris, Simmonds, & Plummer, 2001; Offerle, Eliasson, Grimmond, & Holmer, 2007), building configuration (Alchapar, Correa, & Canton, 2014; Coseo & Larsen, 2014; Monaghan, Hu, Brunsell, Barlage, & Wilhelmi, 2014), and impervious surface area (Imhoff, Zhang, Wolfe, & Bounoua, 2010; Zhang, Imhoff, Wolfe, & Bounoua, 2010). Fundamentally, UHI is a direct consequence of human-induced land surface modifications (Oke, 1995). Linking surface urban/vegetation area to near-surface temperature should provide a robust estimation of human impact and is able to capture the fundamental features of UHI, because the thermal/physical properties of human-made and natural surfaces directly alter the energy budget and flux partitioning.

We come up with a new concept to quantify the UHI, "urban heat island curve (UHIC)", which is designed to explore the spatial relationship between air temperature and urban fraction. Urban fraction is an integrated indicator to show the intensiveness of human activities in a sub-grid scale, usually associated with other urban physical/social factors, such as land use type, surface material, building density and human activities. Although urban fraction is simplified from many surface forcing impacting UHI, it is relatively easy to quantify and meaningful at a larger scale. For finer quantification of UHI, other indicators may be preferred.

Air temperatures were grouped into different urban fraction categories. The urban fraction within a 5 km pixel is simply calculated from the ratio of the urban land cover pixels (MCD12Q1) to the total pixels at 500 m. Land cover in 2012 was used for statistics in 2013 due to unavailable data. We exclude pixels with water bodies because of the strong thermal properties of water, which may skew the trend, especially for the areas near large bodies of water. UHIC is the curve connecting either the median or mean temperature in each urban fraction category.

In this study, we use the median temperature of each urban fraction category as the curve, and also adopt the 25% and 75% quantiles to illustrate the temperature variation. Compared to the mean and standard deviation as statistic indicators, the quantiles can effectively limit the impact of extreme heat events to the curve for presenting a long-term trend.

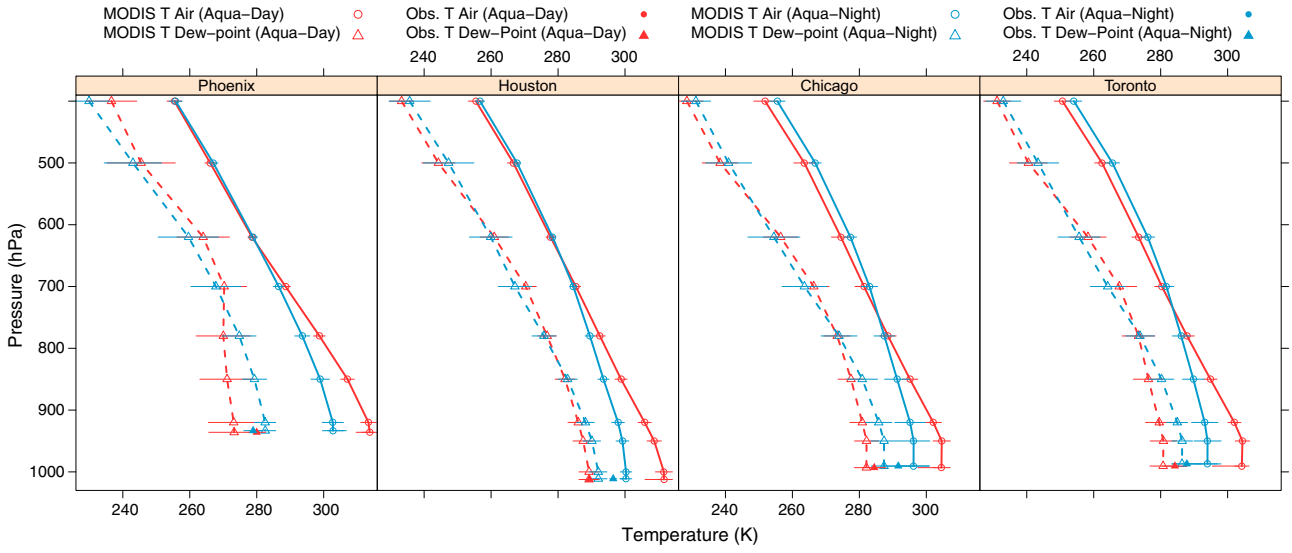

Fig. 2. The mean air temperature and dew-point temperature profiles of an urban pixel for each city. An urban pixel is selected with a ground station with the largest urban fraction in a 5 km pixel. All the profiles were under clear sky conditions in the entire area. The horizontal error bars indicate 1 standard deviation from the mean. Red lines illustrate the state at the Aqua daytime overpass while blue lines correspond to the Aqua nighttime overpass. The solid lines represent air temperature and dashed lines are for dew-point temperature.

4. Results

4.1. Spatial patterns of MODIS near-surface air and dew-point temperature

In order to investigate the ability of MODIS near-surface temperature over the urban area, spatial averages of the 11-years of air and dew-point temperatures are illustrated in Figs. 3 and 4, respectively. The figures portray the averaged day and night satellite overpasses in the UHI diurnal cycle over the four metropolitan areas. In general, MODIS air and dew-point temperatures suggest a remarkable, fine-scale thermal heterogeneity of near-surface features during both daytime and nighttime.

UHI intensities vary spatially and temporally. For Phoenix, the dry environmental background around the urban area decreases the contrast of UHI boundary and temperature variations within the city. However, the major urban area did have relatively higher temperatures than the surroundings and lower than the desert in the southwest corner. Houston shows a strong urban/rural temperature contrast during the daytime while it becomes less distinct at night. Chicago and Toronto demonstrate a very similar diurnal UHI pattern: distinct UHI for both day and night. The quantification of UHI through time and space is discussed in Section 4.3.

The urban effect has less influence on the dew-point temperature before noon (Terra-Day in Fig. 4). It is commonly true that the urban

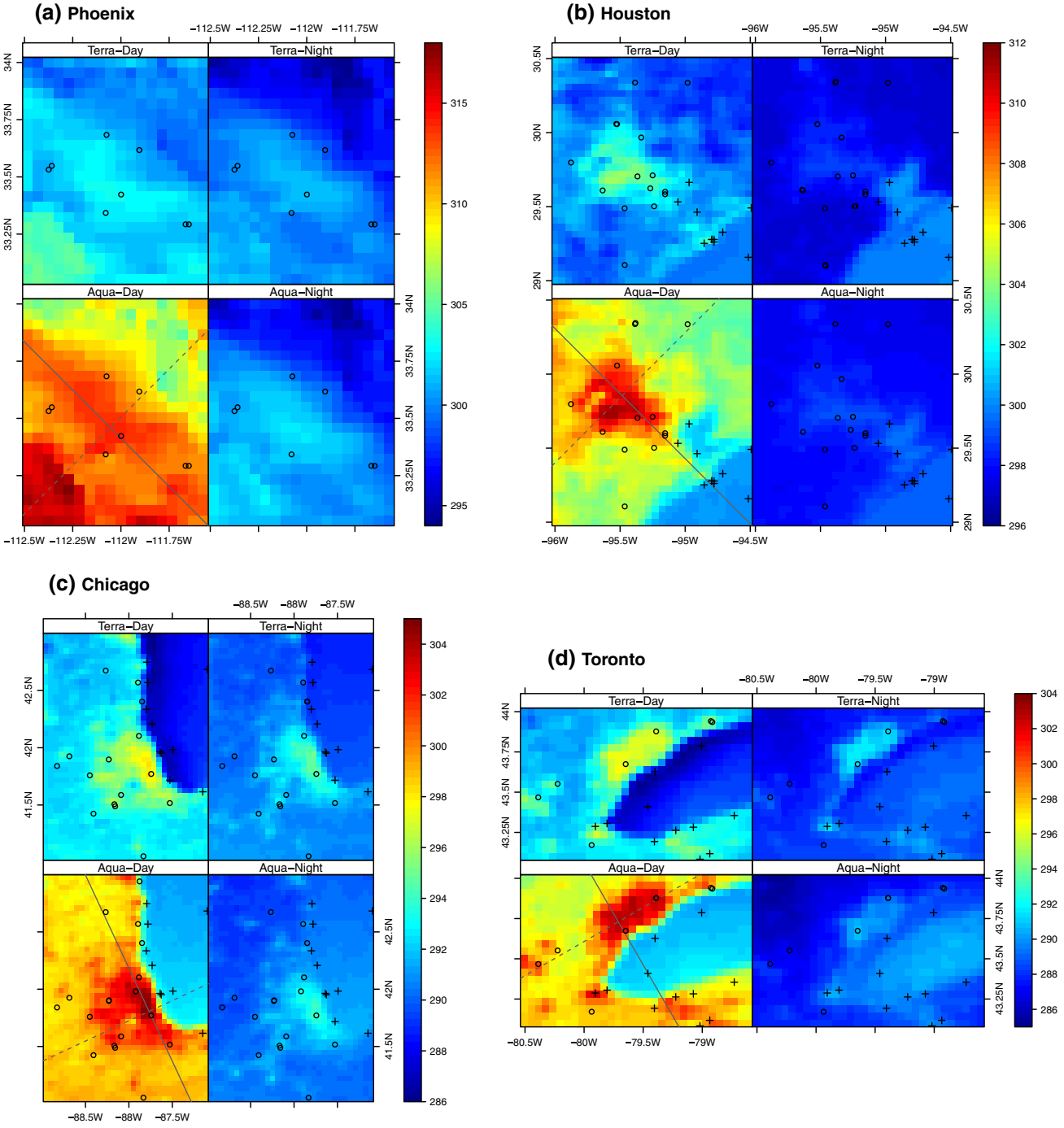

Fig. 3. The 11-year JJA mean near-surface air temperature (T_a^S) of four cities with the hourly ground observation locations. The unfilled circle indicates the sites in 5 km pixels without water fraction. The black cross indicates the sites with water fraction in the pixel. The two gray lines in the Aqua-Day image depict the transect lines for Fig. 7, where a solid line is Transect 1 and a dashed line is Transect 2.

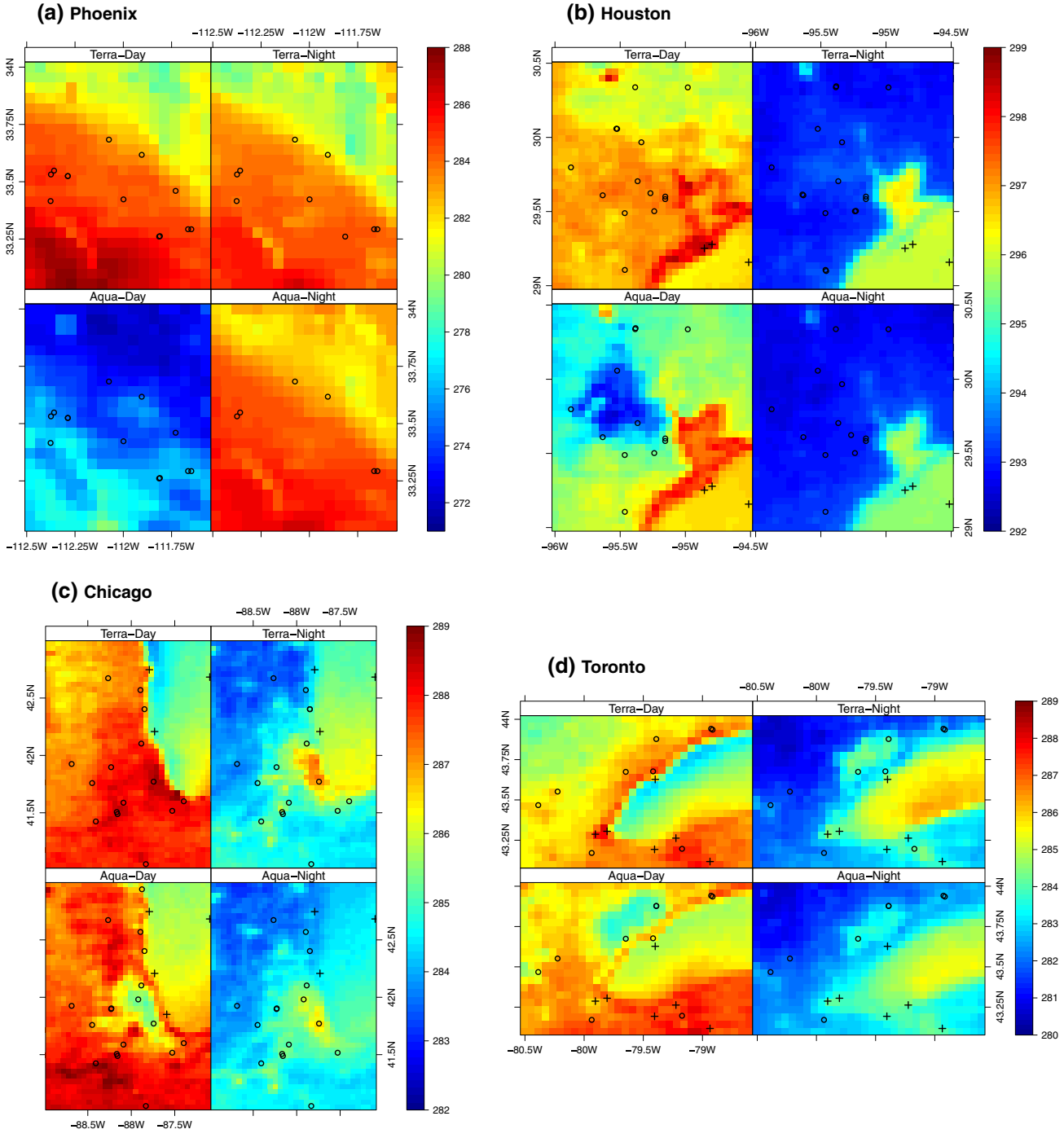

Fig. 4. The 11-year JJA mean near-surface dew-point temperature (T_d^s) of the four cities with hourly ground observation locations.

surface becomes drier in the afternoon due to the urban surface properties (e.g. imperviousness, structure, and thermal properties), limiting the ability to maintain surface moisture and leading to the accumulation of additional energy and anthropogenic heat emissions in the urban canyons. Moreover, the deeper convection developing in the afternoon accelerates moisture dissipation. Consequently, cities usually have a moisture deficit (see Fig. 4 and Fig. S1), evident by high air temperature and low dew-point temperature over the urban area by the time of the Aqua-Day overpass. The nighttime urban area is more humid than the rural surroundings in Toronto and Chicago, showing higher dew-point temperatures. It is commonly observed during clear and calm summer nights and known as nocturnal urban moisture excess (UME) (Kuttler, Weber, Schonnefeld, & Hesselschwerdt, 2007; Tapper, 1990). UME is generally a result of multiple contributions: continued evaporation (Hage, 1975), reduced condensation (Holmer & Eliasson, 1999), rural–urban advection (Haeger-Eugensson & Holmer, 1999), anthropogenic emission of water vapor, etc. There are smaller dew-point temperature gradients between urban and rural area for Phoenix and Houston due to the prevailing dry/wet climate features. The relative humidity over these two urban areas are slightly higher than the ambient rural area (Fig. S1).

In order to assess the overall accuracy of MODIS-retrieved near-surface temperature, the ground observations selected within ±1 h of

each satellite overpass time were directly compared with the corresponding MODIS air temperatures under clear-sky conditions during the 11 summers. Fig. 5 shows the distribution of air temperatures from satellite and surface observations for the four cities. The results of dew-point temperature are similar and can be found in Fig. S2. The sites shown in the scatter plots include the locations over the urban and rural area without water in the 5 km pixel (unfilled circles in Fig. 3). The statistics of MODIS and ground observation comparisons over three categories of site locations are presented in Fig. 6, including sites in a 5 km pixel with urban area but no water surfaces, sites in a 5 km pixel over the land but no water surfaces, and all the sites in each study domain (including urban, rural and water surfaces) (all sites shown in Fig. 3). The urban, rural and water surfaces are determined by the MCD12Q1 yearly land cover data.

Fig. 6 indicates that MODIS air and dew-point temperatures are generally underestimated. For air temperature, Aqua data show a better agreement with the ground observations than Terra, which is about 1–6 K smaller than Terra for the Mean of Differences (MD). In general, nighttime air temperatures agree better than the daytime. Although the RMSE ranges from 3 to 7 K, most instances of very high RMSE are due to the total bias which can potentially be reduced through a correction factor. In contrast to the air temperature, the daytime dew-point temperature comparison generally shows a better agreement, with daytime RMSEs of about 0.3–2.2 K smaller than nighttime RMSEs.

In general, the results of the cities under very dry or humid climate conditions suggest a poorer detectability of MODIS retrievals or larger errors, which may result in more challenges to correct for these effects. For example, the slope of the linear regression between MODIS and ground observations are significantly different from 1 for the nighttime dew-point temperature in Phoenix. The detectability of MODIS for moisture is reduced when the dew-point temperature is low (see Fig. S2), approximately ranging from 260 to 280 K. In Houston, the temperature variation is small for each satellite overpass period with a less clustered distribution in relation to the reference line in Fig. 5. This

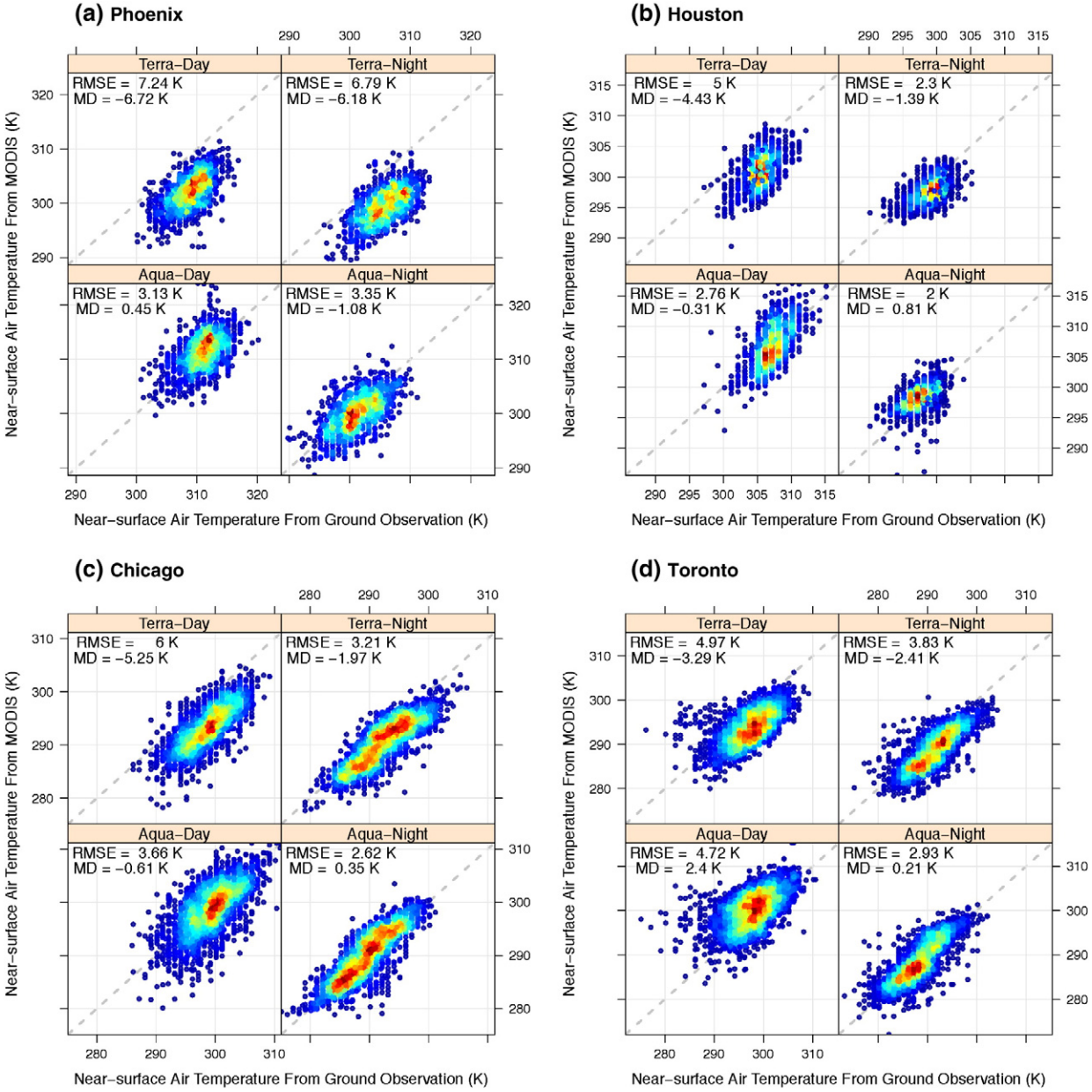

Fig. 5. The density scatter plot of near-surface air temperature from ground observations (the sites denoted as unfilled circles in Fig. 3) and the MODIS product. The point density from low to high is expressed as the color ramp from blue to red. RMSE is the Root-Mean-Square Error, and MD is the Mean of the Differences between MODIS estimations and ground observations in K.

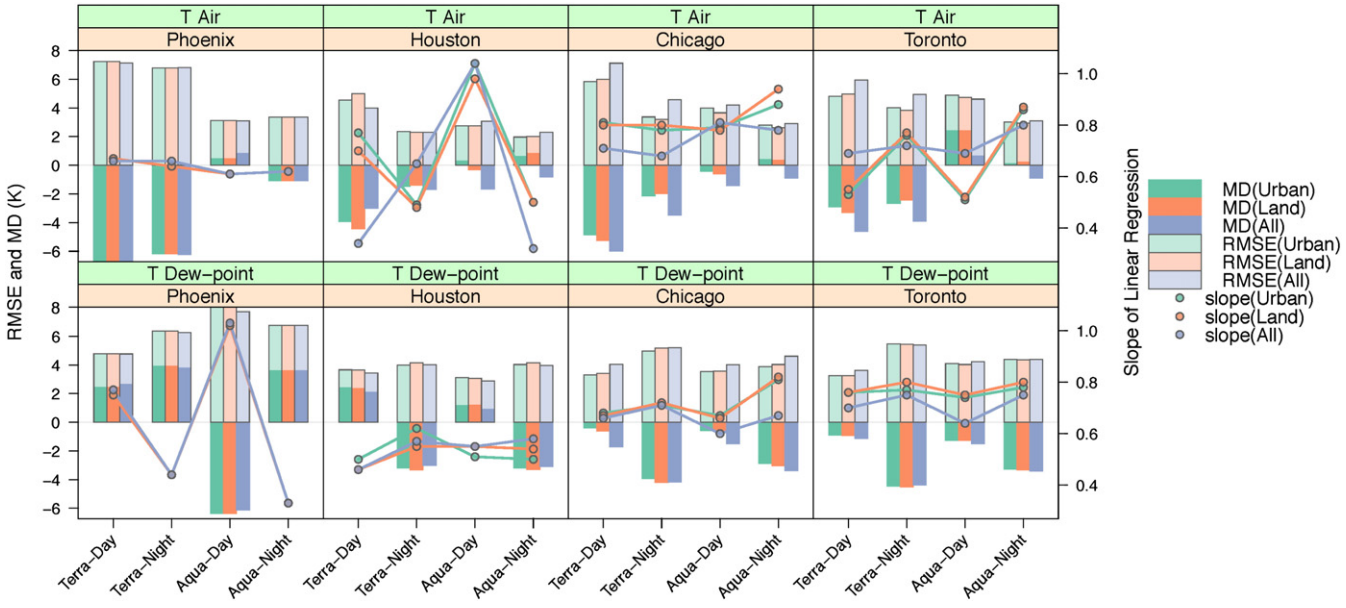

Fig. 6. The Root-Mean-Square Error (RMSE), Mean of the Differences (MD), and the slope of the linear regression between the ground observations and MODIS estimations for three site categories: sites in a 5 km pixel with urban fraction (no water fraction), sites in a 5 km pixel of land surface (no water fraction), and sites in the domain. The near-surface air temperature is shown in the upper-panel plot, and the near-surface dew-point temperature is in the lower row.

possibly explains the large variation of linear regression slopes in Fig. 6. Although the RMSE and MD are sometimes even smaller than other cities, the degree of inaccuracy is difficult to reduce after the corrections. Relatively large air temperature differences exist for Terra, and the dew-point temperature biases occur during the nighttime, so some necessary corrections regarding the observations may need to be applied.

However, the factors related to the mismatch of spatial scale, surface heterogeneity, as well as the possible 1 h observational temporal gap need to be taken into account for the error. Also, the uncertainty in the measurement height will impact the results of the comparison.

This research is attempting to illustrate the applicability of MODIS atmospheric profile product for UHI studies, and the temperature gradients are more emphasized than the absolute temperature magnitude. Consequently, no data correction is provided in this study. The following analysis of the vertical temperature structures and UHIC will focus on Aqua air temperature, which has relatively high accuracy.

4.2. Vertical structure of UHI

The 3-dimensional temperature field may help advance our understanding of the impact of urban surfaces on the lower layers of the atmosphere. Although the vertical resolution of MODIS profiles is relatively coarse, the average summer temperature structures can represent the typical urban climatology for the four cites due to the large data size. Fig. 7 illustrates the 11-year JJA mean vertical air temperature distributions along two orthogonal transects (shown in Fig. 3 Aqua-Day) for each city. The daily atmospheric profiles and near-surface air temperatures were interpolated into 50 m vertical resolution by cubic spline interpolation, and then averaged for the 11 summers. Only Aqua data are plotted here due to the higher quality of near-surface air temperature, and the Aqua daytime period is also closest to the maximum temperature during the day.

The vertical temperature structure reflects the dramatic impact of surface heating extending into the lower-level atmosphere (Fig. 7). The horizontal temperature gradient is interrupted by the change of hot or cool locations with different land cover compositions. One transect of each city is coincident with dominant wind direction. According to the land cover distribution along the transects, the heat distribution in the downwind (sea/lake breezes) directions is evidence of advection during the daytime.

Phoenix is the only inland city in this study with a relatively flat terrain in the urban area and mountains around the city in the domain. Transect 1 and Transect 2 (gray dashed line in Fig. 3) are coincident with the dominant wind direction at Aqua-Night and Aqua-Day, respectively. Multiple factors, such as elevation and land cover distributions, including vegetation, urban and desert, play essential roles impacting UHI features. Although the desert at the southwest corner of the domain (western portion of the Transect 2) has a higher temperature, the heat from the urban area could still be detected due to the relatively lower temperature in the area transitioning from vegetation and higher elevation (Fig. 7(a) Transect 2). For the other three cities near water bodies, the shapes of the heat dome have a relatively clear boundary associated with the surface land cover types.

4.3. Application of MODIS air temperature for UHI assessment–urban heat island curve

With the spatial distribution of summer air temperature for 11 years, the urban heat island curves (UHIC) are shown in Fig. 8 for the four cities and four satellite-overpass periods. The 25%, 50% and 75% quantiles of air temperature for each group of urban fraction reveal a city-dependent temperature trend. The median of air temperatures of fully vegetated pixels is added as a reference line (gray dashed line in Fig. 8). The data from the Terra overpass showed a low bias (about 3.3–6.7 K for daytime and 1.4–6.2 K for nighttime) compared to the ground observations (in Section 4.1). With an assumption that the bias is spatially consistent, the shape of the UHIC and the difference between the UHIC and the fully vegetated temperature line are less impacted by the total bias of MODIS air temperature.

Compared with pairs of urban–rural temperature differences, the UHIC incorporates the spatial heterogeneity of the whole city domain in the curve, resulting in a unique pattern for each city. The air temperature showed a positive slope as a function of urban fraction. The magnitude of the slope varied temporally and spatially. For example, the air temperature differences among the pixels with 60% and higher urban fraction in Phoenix were small, which is related to the local climate and vegetation types in the non-urban fraction. However, a positive

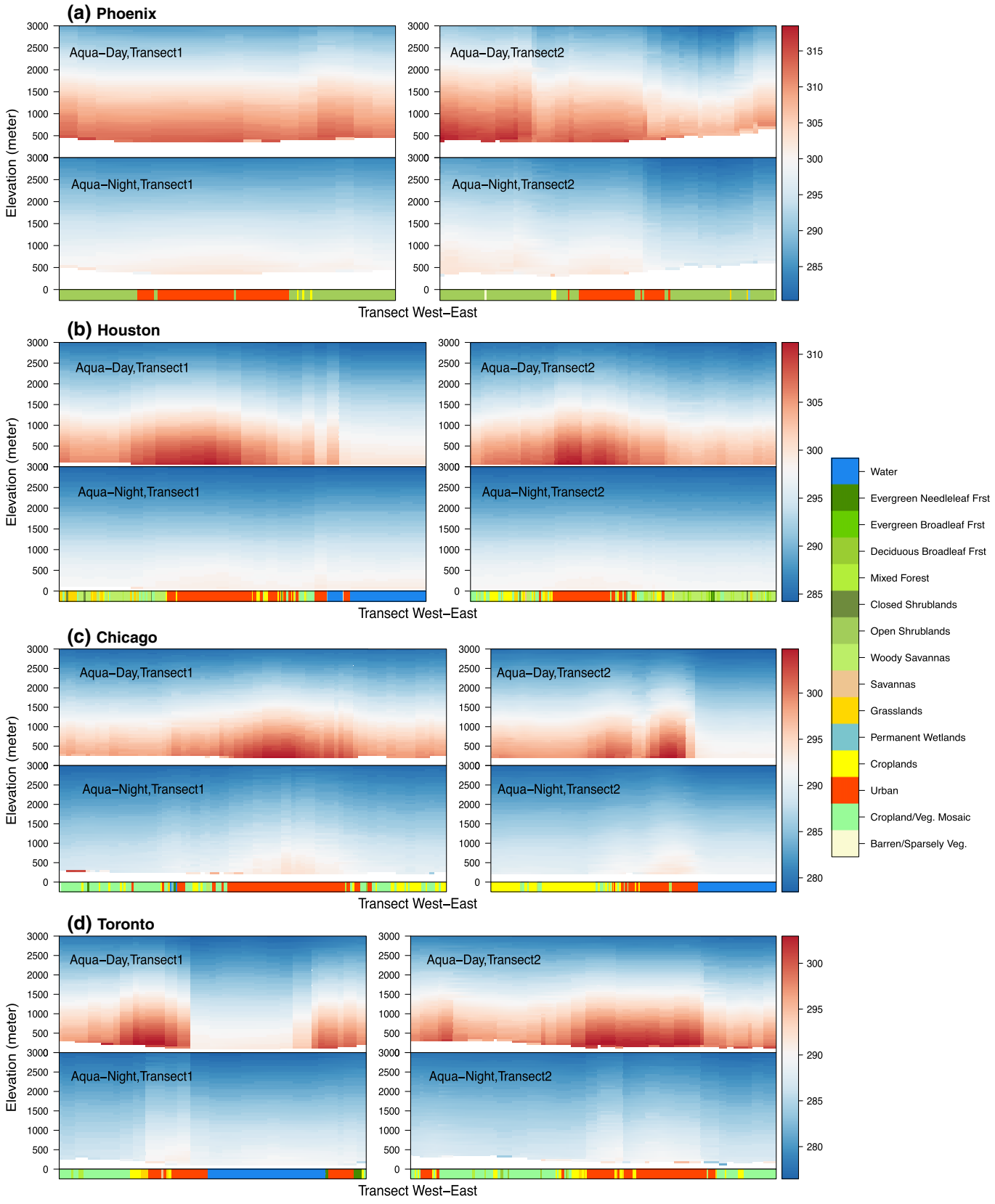

Fig. 7. The mean vertical temperature distributions from Aqua distribution along two orthogonal horizontal transects for both day and night conditions for the four cities. The bottom color bar indicates corresponding land cover types along the transects. The white area at the bottom represents the ground below the surface elevation.

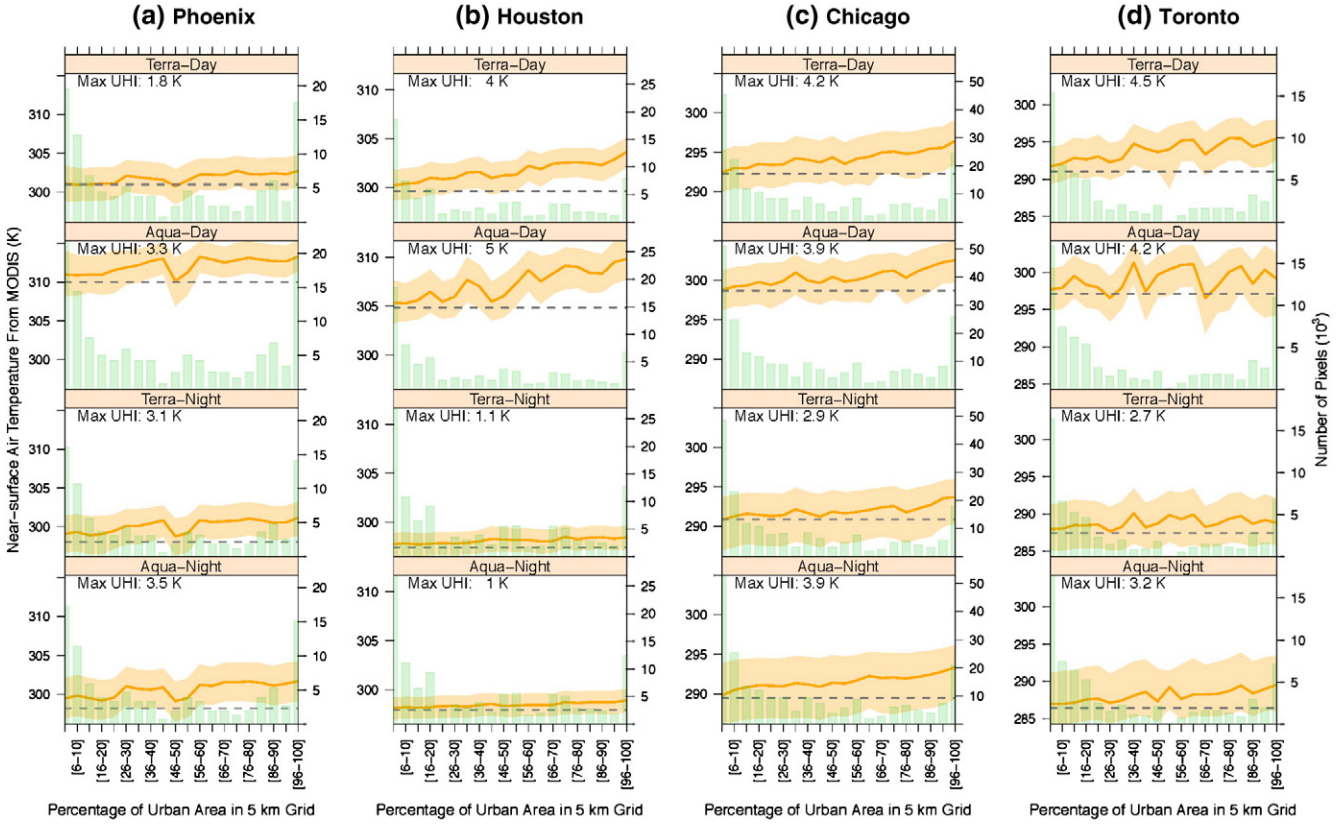

Fig. 8. The UHIC of four cities as a function of urban fraction (at 5% interval) in 5 km pixel using 2003–2013 JJA data. The solid orange line is the median air temperature of the pixels with corresponding urban fractions (left y-axis). The shaded orange area indicates the 25% and 75% quantiles of the air temperature distributions (left y-axis). The gray dashed line represents the mean air temperature over the fully-vegetated pixels in each city. Max UHI is the difference between the highest median air temperature on the UHIC and mean vegetation temperature. The light green bar plot (right y-axis) shows the number of pixels in each group used in the calculation of the 11 year summer statistics.

slope was observed among the lower urban fraction groups (1%–45%). In the Greater Houston, the UHIC slope became very steep during the daytime (about 3.0 for Terra-Day, and 4.6 for Aqua-Day), suggesting a large impact of the urban surface that contributes to the higher air temperature. Comparably, the nighttime UHIC of Houston increased steadily and slowly, with the slopes of 0.8 and 0.7 for Terra and Aqua night, respectively. The UHICs of Chicago have relatively similar steep positive slopes for both day and night, ranging from 2.1 to 3.2. There is a large variation of Toronto Aqua-Day UHIC; however, the trend was still positive with a slope of 1.85. Other times of day for Toronto revealed a steady increase (with a slope of 3.5) in temperature with increasing urban fraction. The large variation may be impacted by some scattered urban areas around the lake in the domain, especially during times with strong fluxes. These results support the widely accepted fact that UHI is primarily caused by the urban modification to the surface energy balance (Stewart & Oke, 2012). Moreover, the UHIC reveals more spatial complexity impacting temperature variations in space and time than other UHI indicators.

The gray dashed line in Fig. 8 presents the median temperature of fully-vegetated pixels in each domain. The dominant vegetation types around the cities are shrublands (Phoenix), croplands and savannas (Houston), croplands (Chicago), and croplands and natural vegetation mosaic (Toronto). The maximum median temperature differences between urban and pure vegetation are also shown in Fig. 8. A comparison between the air temperature with low urban fractions and the pure-vegetation temperature showed a slightly different magnitude in most cases, which can be explained by the influence of the urban fraction as well as the ambient pixels when considering the clustered pattern of urban surfaces. The majority of urban pixels at the 5 km resolution are a composite of urban and vegetation. Pixels with water fraction are not considered in the UHIC. However, pixels with urban fraction in Phoenix may also consist of the barren soil, which increases the temperature difference from the fully-vegetated pixels.

In general, the UHIC varies from city to city during the same satellite overpass period. The variability is largely determined by the land use pattern in both urban and non-urban fractions in each city. Sometimes, UHIC is more complex than simple increasing, where the surface properties in non-urban fractions play important roles, e.g. urban forest, irrigated lawn, or bare soil. Monaghan et al. (2014) demonstrated the significance of urban/vegetation fraction and irrigation on the temperature by a modeling method. For example, a drop in the UHIC (e.g. Aqua-day overpass in Phoenix at 46%–50% urban fraction) showing a higher urban fraction area with lower air temperature, may be a result of one or multiple inexplicit reasons. If the elevation, building types and heights are homogeneous across the space, the vegetation types and the irrigation management in the non-urban fraction, and the surrounding land cover types (parks versus industrial) are usually key factors. Also, for the urban fraction higher than 56% in Phoenix, the temperature changes become very small, indicating that the lack of vegetated area in the urban area decreases the impact of urban fraction size on the air temperature in the 5 km grid. Moreover, each city has similar UHIC shapes with a different magnitude of variation at four satellite overpass times, which highlights how various surface components respond to the heating/cooling process. In general, the Aqua-Day (early afternoon) reveals the largest variation while UHIC is smoother during nighttime.

The light-green bars (right y-axis) in Fig. 8 illustrate the number of pixels in each urban fraction category. This value accounts for two main factors: the number of pixels with a certain urban fraction in each city and the number of clear days for 11-year JJA. The “U-shape” distribution of pixel numbers along with the urban fraction increasing may depict the urban density decreasing from the urban core. Heterogeneity in the cloud distribution over the study area also impacts the

sample size. In general, the higher urban density is more likely to be cloudy due to the strong convection during the late afternoon (Hu & Brunsell, 2013). For some coastal cities, some parts of the most highly developed areas are likely less cloudy due to the sea/lake breeze effect. The UHIC is based on robust statistics for the 11-year summers under clear-sky conditions. Some attention needs to be paid to the categories with relatively small sample sizes, e.g. 75 for Terra-Night and 93 for Aqua-Night with urban fractions of 51%–55% in Toronto. This may decrease the confidence level of the variation in the UHIC.

The dew-point temperature is also applied to UHIC method, shown in Fig. S3. A decreasing trend of humidity is associated with an increase in urban fraction during the Aqua daytime overpass in all cities except Phoenix. Phoenix has less evapotranspiration in both non-urban fraction parts and rural areas, resulting in little variation of UHIC from dew-point temperature. A higher nocturnal UME is observed in areas with higher urban fractions especially in Chicago and Toronto. UME also happens in the summer mornings (Terra-Day) in most cases. Fig. 9 shows the correlation coefficients of air temperature and dew-point temperature on UHIC. The result suggests a statistically significant positive relationship between temperature and moisture spatially in Chicago, Toronto and Phoenix during nighttime overpasses. However, spatial heterogeneity of nocturnal UME was observed in Houston probably due to the moist sea breeze (Day, Rappenglck, Clements, Tucker, & Alan Brewer, 2010). The moisture deficit found in the afternoon is also highly related to the temperature increment in the urban area, with a significant and strong negative correlation.

5. Discussion

As is widely known, MODIS is not designed for sounding purposes. However, the information provided at high spatial resolution can "improve upon a priori definitions of atmospheric state by providing better delineation of horizontal gradients (King et al., 2003)." MODIS-derived air and dew-point temperatures in this study show an ability to capture the heat distributions in three dimensions. The availability of the near-surface air temperature solves the problems of limited numbers and footprints of ground-based observations in the urban area for atmospheric UHI research. Comparison of MODIS-derived temperatures with ground observations shows fairly good results.

The near-surface air temperatures derived from the profiles are more likely to be above UCL and at the base height of UBL. Oke (1976) discussed two different concepts regarding UCL and UBL UHIs. UCL describes the climate features impacted by the urban roughness elements at a microscale, while the urban boundary layer is dominated by urban area and its lower boundary at a local or mesoscale. The signal sensed from the urban surface includes roof, wall, and ground depending on the view angles. Further, the retrieval of the near-surface temperature is determined by the mean elevation within a 5 km pixel. The height representing the MODIS air temperature at 5 km resolution may diminish the influence of building/canopy height variations and enhance the terrain impact at this scale. Fortunately, most cities are located in flat terrain, so the estimated height is more likely to be in the top or above the UCL in general. In more mountainous regions, in addition to the land-cover forcing, the terrain impacts may introduce more complicating factors that influence the temperature.

The MODIS atmospheric profile product is derived from the integrated information of cloud-free instantaneous field-of-views (IFOVs) at 1 km within 5×5 km area. Therefore, sunny areas may lead to more reliable estimations. Urban areas tend to be more cloudy in general (Rabin & Martin, 1996). The number of clear sky pixels for satellite overpasses during the study period suggests more cloudy summers in the Houston area compared to the other three cities (see Fig, S4). One reason for more clouds over the urban areas is that the deep convection happens in the afternoon enhancing the chance of clouds (Angevine et al., 2003). Also, anthropogenic emissions provide additional sources of cloud condensation nuclei. The frequent presence of clouds over the Greater Houston area potentially decreases the number of cloud-free IFOVs at the 5 km scale. This may explain the relatively low correlation coefficients and large variations of slopes of linear regressions between the MODIS estimations and ground observations. Similarly, the sky conditions of the ground observations may not represent the clear-sky pixels of MODIS. Some other factors, such as the presence of significant advective influences in Houston, are also potential reasons for the errors. More precise experiments may be needed to further evaluate the accuracy of MODIS-derived air temperature over very cloudy cities.

The diurnal UHI patterns illustrated in Figs. 3 and 8 for some cities are slightly different from the features of atmospheric UHI and surface UHI. Pronounced atmospheric UHI effects are usually found under calm and clear nights (Voogt & Oke, 2003), which is related to the different heating/cooling rates over urban and rural surfaces (Oke, 1982). The SUHIs usually exhibit stronger and larger spatial variability during the daytime (Hu & Brunsell, 2013; Hung, Uchihama, Ochi, & Yasuoka, 2006; Roth, Oke, & Emery, 1989). Fig. 10 gives a broad idea of the diurnal cycle of all the ground sites in each city illustrated with four satellite overpass periods. The temperature range over the study area at a particular time indicates a temperature variation due to different land surface properties, which can be a rough UHI magnitude. However, the environment of the ground sites varies in each city. The choice of urban/rural sites is critical in determining the UHI magnitude. We should realize that the ground measurements at the "urban" and "rural" sites only illustrate one possible UHI intensity, which may represent one point on the UHIC. The maximum UHI described in Fig. 8 has an emphasis on

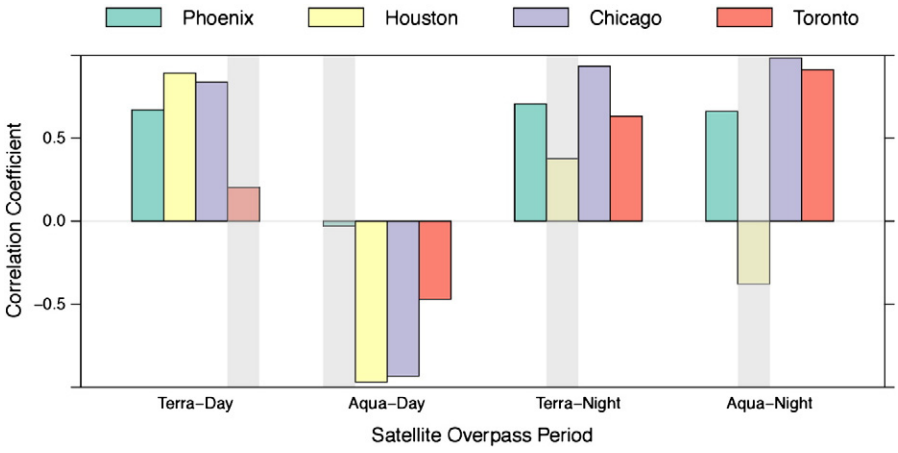

Fig. 9. The correlation coefficients of UHIC for air temperature and dew-point temperature. The light gray shaded area indicates that the relationship is not statistically significant at $p = 0.05$.

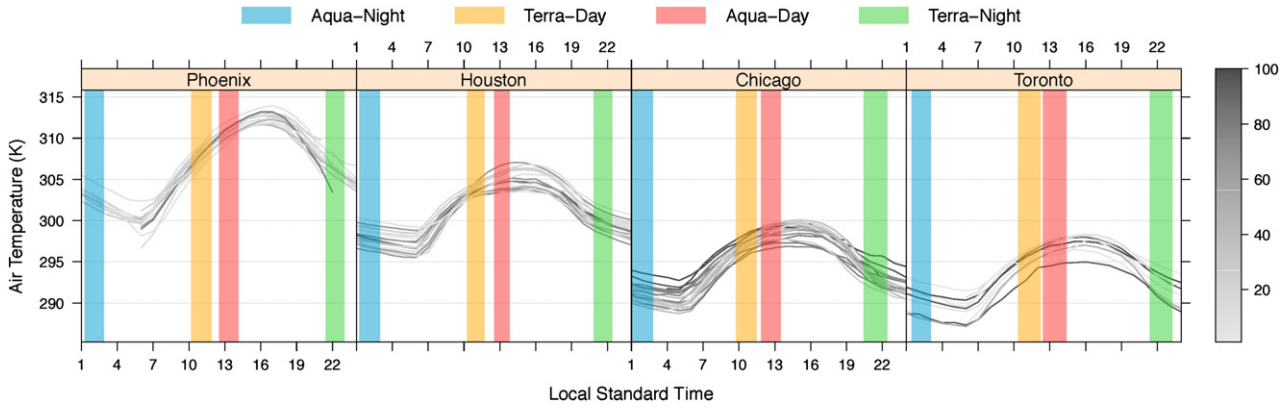

Fig. 10. The mean diurnal cycles of each site (gray-scale) over the urban/rural areas shown as unfilled circles in Fig. 3. The range of gray lines indicates the temperature difference across the space. The gray-scale indicates the urban fraction (%) from 1 (light gray) to 100 (dark). Four satellite overpass periods are shaded in four colors.

urban/vegetation temperature differences at one time across space, which is different from the common concept of maximum UHI in a diurnal cycle that usually occurs after sunset (Bohnenstengel, Evans, Clark, & Belcher, 2011) and is determined by observations from a pair of urban and rural stations. Houston shows a lower UHI from nighttime MODIS, which may be related to the rural temperature definition and the integration of all the vegetation on the land and near the ocean. Humid environments decrease the sensitivity of MODIS performance (see Figs. 5 and S2), as well as an increasing uncertainty (see Fig. S4) in Houston due to more frequent cloud cover. For most cases, the daytime UHI is slightly enhanced compared to nighttime for the atmospheric UHI. One possible reason is that the regression statistics algorithm is based on the signals detected from a narrow solid angle of view from the sensor at different zenith view angles ranging from −65° to +65°. The observed surface components impact the representativeness of the near-surface temperatures. Also, the near-surface temperature from MODIS represents a higher height rather than screen level.

When concerning human health and living environments in the urban area, the air temperatures are potentially better sources compared with the LST. The research for SUHI spatiotemporal dynamics and the techniques for spatial/temporal scaling can also apply to air temperature. Furthermore, the overpass time of Aqua-Day is closest to the time of the maximum air temperature. With the availability of both air and dew-point temperatures, MODIS can be an invaluable source to conduct heat stress studies at a larger scale, which may require further correction. For example, time-based corrections of MODIS estimated near-surface temperatures may need to be applied using the diurnal temperature pattern from other high temporal-frequency data, such as in-situ observations. Moreover, the time variation should be considered based on the day-to-day corrections. Other factors, such as the influence of roofs, the mean radiant temperature of surroundings as a loading on humans also need careful consideration.

Compared to the common UHI indicators in the literature (Schwarz et al., 2011), the UHIC has many advantages. 1) UHIC integrates the urban surface heterogeneity, which also avoids the biases caused by urban/rural divisions. 2) UHIC can capture the urban surface features; consequently, each city has a unique UHIC. 3) UHIC can be constructed for different temporal scales, such as annual, seasonal, and diurnal scales. 4) UHIC is universal and easy to use for comparisons across time and space. 5) UHIC is less influenced by the bias of the data source, due to the reliance on the gradients rather than absolute values of temperatures.

There are some caveats for the applications of UHIC. The urban fractions integrate many inexplicit factors. For example, the urban fraction is highly correlated to the major urban land use types. The different local climate zones (Stewart & Oke, 2012) with similar urban fraction but a quite large variety of building configuration and terrain roughness may diverge from the temperature distributions. For such situations, UHIC only shows the integrated results. A particular region is likely to contain only a few local climate zones, because the urban features usually are highly correlated due to the close geolocations, similar climate, shared cultural and economic settings. The UHIC should be interpreted city by city among different regions. The non-urban fraction, such as water bodies, dense vegetation and barren soil, also plays a critical role in the air temperature over the urban area. Other possible solutions include using impervious surface area or other parameters that could distinguish urban features heavily impacting the temperature instead of the urban fraction.

The urban fraction is a relative concept according to the source resolution to distinguish the urban surfaces and target scale to calculate the fraction. In this study, we employed the urban pixels at 500 m for UHIC, which is defined by the dominant built areas larger than 50% in the 500 m pixel and the contiguous patches of urban environment larger than 1 km^2 (Schneider, Friedl, & Potere, 2009). The urban built-up area within each pixel varies widely around the world and is influenced by many social and climatic factors (Friedl et al., 2010). The higher resolution of land cover data will naturally decrease the non-urban fraction mixed in the upscaled pixel level. The proper ratio of resolutions for the upscaling and statistics should be determined by the quantifying interval of the urban fraction, such as 5% in this study, and the accuracy requirement.

UHIC under clear-sky conditions can be applied to different temporal scales but is sensitive to the time of day (Fig. 8). In order to guarantee sufficient sample size, monthly or seasonal UHICs are preferred for relatively longer observations for the cloudy areas. Finally, the UHIC is not a single-value UHI indicator, but it helps estimate other indicators, such as intra-urban (e.g. urban core versus parks) and urban–rural (e.g. urban core versus water, cropland, or other rural area as a whole) temperature differences.

6. Conclusions

By estimating the near-surface air and dew-point temperatures from the MODIS atmospheric profile product (MOD07_L2), this is the first study that exploits the ability of MODIS to capture the temporal dynamics, and spatial structures (horizontal and vertical) of atmospheric UHI for four mega cities in North America during 2003–2013 summers. In addition, this study develops an UHI curve to represent UHI intensity by integrating the urban surface heterogeneity in a curve, showing the relationship between the air temperature and the urban fractions. Also, this study tests the relationship between temperature and moisture based on the UHIC.

MODIS atmospheric profile data are an invaluable source to capture the urban thermal distributions in horizontal (5 km), vertical (20

pressure levels) and temporal (4 times a day) dimensions. The MODIS near-surface temperature represents an integrated result in a 5 km grid, including urban morphology, surface material heterogeneity, terrain, solar angle, and sensor view angle. The comparison between the MODIS near-surface temperature and the ground observations suggests an accuracy of 3–7 K RMSE for different cities and times of day. In general, very dry and moist climate conditions increase the variability of the MODIS temperature accuracy. Although the magnitude seems relatively high, it can be reduced by correcting for the total biases.

The MODIS air temperature provides a less expensive way to conduct UHI research and is able to capture the fine-scale gradients over the complex urban areas due to the relatively high spatial resolution. UHIC provides a new way to quantify UHI city by city, which emphasizes the temperature gradients for different urban fractions, consequently decreasing the impact of the data biases.

This study evaluates the performance of MODIS air and dew-point temperatures during summer months. Further evaluations will be worthwhile for other seasons, as well as for other cities in different regions under various climatic conditions. Moreover, this study presents the original MODIS temperature and its application for UHIC under basic quality controls and does not discuss any correction method in detail or use corrected results. Simple linear regression between MODIS data and observations, possibly, is the easiest way to correct the primary bias. Systematic research may be required to limit the bias and to control the uncertainty for other applications that depend on the absolute magnitude of air and dew-point temperatures.

Acknowledgments

This work was supported under the National Aeronautics and Space Administration program (NNX10AK79G). We would like to thank Dr. David Mechem and Dr. David Rahn for the useful comments on the manuscript. Thanks are also due to Dr. Abe Taaheri who provided the technical supports of HEG software.

Appendix A. Supplementary data

Supplementary data to this article can be found online at http://dx.doi.org/10.1016/j.rse.2014.10.022.

References

Alchapar, N. L., Correa, E. N., & Canton, M. A. (2014). Classification of building materials used in the urban envelopes according to their capacity for mitigation of the urban heat island in semiarid zones. *Energy and Buildings*, *69*, 22–32.

Angevine, W. M., White, A. B., Senff, C. J., Trainer, M., Banta, R. M., & Ayoub, M. A. (2003). Urban–rural contrasts in mixing height and cloudiness over Nashville in 1999. *Journal of Geophysical Research-Atmospheres*, *108*(D3).

Aumann, H. H., Chahine, M. T., Gautier, C., Goldberg, M. D., Kalnay, E., McMillin, L. M., et al. (2003). AIRS/AMSU/HSB on the Aqua mission: Design, science objectives, data products, and processing systems. *Geoscience and Remote Sensing, IEEE Transactions on*, *41*(2), 253–264.

Barlow, J. F., Dunbar, T. M., Nemitz, E. G., Wood, C. R., Gallagher, M. W., Davies, F., et al. (2011). Boundary layer dynamics over London, UK, as observed using Doppler lidar during REPARTEE-II. *Atmospheric Chemistry and Physics*, *11*(5), 2111–2125.

Bisht, G., & Bras, R. L. (2010). Estimation of net radiation from the MODIS data under all sky conditions: Southern Great Plains case study. *Remote Sensing of Environment*, *114*(7), 1522–1534.

Bisht, G., Venturini, V., Islam, S., & Jiang, L. (2005). Estimation of the net radiation using MODIS (Moderate Resolution Imaging Spectroradiometer) data for clear sky days. *Remote Sensing of Environment*, *97*(1), 52–67.

Bohnenstengel, S., Evans, S., Clark, P. A., & Belcher, S. (2011). Simulations of the London urban heat island. *Quarterly Journal of the Royal Meteorological Society*, *137*(659), 1625–1640.

Borbas, E., Seemann, S. W., Kern, A., Moy, L., Li, J., Gumley, L., et al. (2011). *MODIS atmospheric profile retrieval algorithm theoretical basis document, collection 6.* Tech. rep., University of Wisconsin-Madison.

Coseo, P., & Larsen, L. (2014). How factors of land use/land cover, building configuration, and adjacent heat sources and sinks explain urban heat islands in Chicago. *Landscape and Urban Planning*, *125*, 117–129.

Day, B. M., Rappenglck, B., Clements, C. B., Tucker, S. C., & Alan Brewer, W. (2010). Nocturnal boundary layer characteristics and land breeze development in Houston, Texas during TexAQS II. *Atmospheric Environment*, *44*(33), 4014–4023.

Friedl, M. A., Sulla-Menashe, D., Tan, B., Schneider, A., Ramankutty, N., Sibley, A., et al. (2010). MODIS collection 5 global land cover: Algorithm refinements and characterization of new datasets. *Remote Sensing of Environment*, *114*(1), 168–182.

Gallo, K. P., Tarpley, J. D., Mcnab, A. L., & Karl, T. R. (1995). Assessment of urban heat islands — A satellite perspective. *Atmospheric Research*, *37*(1–3), 37–43.

Grimmond, C. S. B. (2006). Progress in measuring and observing the urban atmosphere. *Theoretical and Applied Climatology*, *84*(1–3), 3–22.

Haeger-Eugensson, M., & Holmer, B. (1999). Advection caused by the urban heat island circulation as a regulating factor on the nocturnal urban heat island. *International Journal of Climatology*, *19*(9), 975–988.

Hage, K. D. (1975). Urban–rural humidity differences. *Journal of Applied Meteorology*, *14*(7), 1277–1283.

Holmer, B., & Eliasson, I. (1999). Urban–rural vapour pressure differences and their role in the development of urban heat islands. *International Journal of Climatology*, *19*(9), 989–1009.

Hu, L., & Brunsell, N. A. (2013). The impact of temporal aggregation of land surface temperature data for surface urban heat island (SUHI) monitoring. *Remote Sensing of Environment*, *134*, 162–174.

Hu, L., Brunsell, N. A., Monaghan, A. J., Barlage, M., & Wilhelmi, O. V. (2014). How can we use MODIS land surface temperature to validate long term urban model simulations? *Journal of Geophysical Research, [Atmospheres]*, *119*(6), 3185–3201.

Hung, T., Uchihama, D., Ochi, S., & Yasuoka, Y. (2006). Assessment with satellite data of the urban heat island effects in Asian mega cities. *International Journal of Applied Earth Observation and Geoinformation*, *8*(1), 34–48.

Imhoff, M. L., Zhang, P., Wolfe, R. E., & Bounoua, L. (2010). Remote sensing of the urban heat island effect across biomes in the continental USA. *Remote Sensing of Environment*, *114*(3), 504–513.

Kalkstein, L. S., & Greene, J. S. (1997). An evaluation of climate/mortality relationships in large US cities and the possible impacts of a climate change. *Environmental Health Perspectives*, *105*(1), 84–93.

Kidd, C., Levizzani, V., & Bauer, P. (2009). A review of satellite meteorology and climatology at the start of the twenty-first century. *Progress in Physical Geography*, *33*(4), 474–489.

Kim, D. Y., & Han, K. S. (2013). Remotely sensed retrieval of midday air temperature considering atmospheric and surface moisture conditions. *International Journal of Remote Sensing*, *34*(1), 247–263.

Kim, J. Y., & Hogue, T. S. (2008). Evaluation of a MODIS-based potential evapotranspiration product at the point scale. *Journal of Hydrometeorology*, *9*(3), 444–460.

King, M. D., Menzel, W. P., Kaufman, Y. J., Tanre, D., Bo-Cai, G., Platnick, S., et al. (2003). Cloud and aerosol properties, precipitable water, and profiles of temperature and water vapor from MODIS. *Geoscience and Remote Sensing, IEEE Transactions on*, *41*(2), 442–458.

Kuttler, W., Weber, S., Schonnefeld, J., & Hesselschwerdt, A. (2007). Urban/rural atmospheric water vapour pressure differences and urban moisture excess in Krefeld, Germany. *International Journal of Climatology*, *27*(14), 2005–2015.

Mage, D., Ozolins, G., Peterson, P., Webster, A., Orthofer, R., Vandeweerd, V., et al. (1996). Urban air pollution in megacities of the world. *Atmospheric Environment*, *30*(5), 681–686.

Menzel, W. P., & Purdom, J. F. W. (1996). Introducing GOES-1: The first of a new generation of geostationary operational environmental satellites. 1. The satellite sensor systems, quality control procedures for converting data into products. *Earth Observation and Remote Sensing*, *14*(1), 81–99.

Monaghan, A. J., Hu, L., Brunsell, N. A., Barlage, M., & Wilhelmi, O. V. (2014). Evaluating the impact of urban morphology configurations on the accuracy of urban canopy model temperature simulations with MODIS. *Journal of Geophysical Research, [Atmospheres]*, *119*(11), 6376–6392.

Morris, C., Simmonds, I., & Plummer, N. (2001). Quantification of the influences of wind and cloud on the nocturnal urban heat island of a large city. *Journal of Applied Meteorology*, *40*(2), 169–182.

NOAA National Ocean Service (2013). *National coastal population report, population trends from 1970 to 2020.* Tech. rep., National Oceanic and Atmospheric Administration, Department of Commerce.

Offerle, B., Eliasson, I., Grimmond, C. S. B., & Holmer, B. (2007). Surface heating in relation to air temperature, wind and turbulence in an urban street canyon. *Boundary-Layer Meteorology*, *122*(2), 273–292.

Oke, T. R. (1976). The distinction between canopy and boundary layer urban heat islands. *Atmosphere*, *14*(4), 268–277.

Oke, T. R. (1982). The energetic basis of the urban heat-island. *Quarterly Journal of the Royal Meteorological Society*, *108*(455), 1–24.

Oke, T. R. (1995). The heat island of the urban boundary layer: Characteristics, causes and effects. In J. Cermak, A. Davenport, E. Plate, & D. Viegas (Eds.), *Wind climate in cities. of NATO ASI Series, vol. 277.* (pp. 81–107). Springer Netherlands.

Oke, T. R. (2008). Urban observations. (7th ed.). *Guide to meteorological instruments and methods of observation, part II observing systems*. Geneva: World Meteorological Organization (Chapter 11, WMO-No.8).

Patz, J. A., Campbell-Lendrum, D., Holloway, T., & Foley, J. A. (2005). Impact of regional climate change on human health. *Nature*, *438*(7066), 310–317.

Rabin, R. M., & Martin, D. W. (1996). Satellite observations of shallow cumulus coverage over the central United States: An exploration of land use impact on cloud cover. *Journal of Geophysical Research-Atmospheres*, *101*(D3), 7149–7155.

Reale, A. L. (2002). NOAA operational sounding products for advanced-TOVS. *NOAA Tech. Rep. NESDIS, vol. 107.* (pp. 29) (Washington D.C.).

Roth, M. (2000). Review of atmospheric turbulence over cities. *Quarterly Journal of the Royal Meteorological Society*, *126*(564), 941–990.

Roth, M., Oke, T. R., & Emery, W. J. (1989). Satellite-derived urban heat islands from 3 coastal cities and the utilization of such data in urban climatology. *International Journal of Remote Sensing*, *10*(11), 1699–1720.

Schneider, A., Friedl, M. A., & Potere, D. (2009). A new map of global urban extent from MODIS satellite data. *Environmental Research Letters*, *4*(4).
Schwarz, N., Lautenbach, S., & Seppelt, R. (2011). Exploring indicators for quantifying surface urban heat islands of European cities with MODIS land surface temperatures. *Remote Sensing of Environment*, *115*(12), 3175–3186.
Seemann, S., Borbas, E. E., Li, J., Menzel, W. P., & Gumley, L. E. (2006). *MODIS atmospheric profile retrieval algorithm theoretical basis document*. Tech. rep.
Seemann, S. W., Li, J., Menzel, W. P., & Gumley, L. E. (2003). Operational retrieval of atmospheric temperature, moisture, and ozone from MODIS infrared radiances. *Journal of Applied Meteorology*, *42*(8), 1072–1091.
Stewart, I. D. (2011). A systematic review and scientific critique of methodology in modern urban heat island literature. *International Journal of Climatology*, *31*(2), 200–217.
Stewart, I. D., & Oke, T. R. (2012). Local climate zones for urban temperature studies. *Bulletin of the American Meteorological Society*, *93*(12), 1879–1900.
Taha, H. (1997). Urban climates and heat islands: Albedo, evapotranspiration, and anthropogenic heat. *Energy and Buildings*, *25*(2), 99–103.
Tapper, N. J. (1990). Urban influences on boundary layer temperature and humidity: Results from Christchurch, New Zealand. *Atmospheric Environment Part B Urban Atmosphere*, *24*(1), 19–27.
Vancutsem, C., Ceccato, P., Dinku, T., & Connor, S. J. (2010). Evaluation of MODIS land surface temperature data to estimate air temperature in different ecosystems over Africa. *Remote Sensing of Environment*, *114*(2), 449–465.
Voogt, J. A., & Oke, T. R. (2003). Thermal remote sensing of urban climates. *Remote Sensing of Environment*, *86*(3), 370–384.
Wang, W. H., & Liang, S. L. (2009). Estimation of high-spatial resolution clear-sky longwave downward and net radiation over land surfaces from MODIS data. *Remote Sensing of Environment*, *113*(4), 745–754.
Weng, Q. H., Lu, D. S., & Schubring, J. (2004). Estimation of land surface temperature–vegetation abundance relationship for urban heat island studies. *Remote Sensing of Environment*, *89*(4), 467–483.
Weng, Q. H., Rajasekar, U., & Hu, X. F. (2011). Modeling urban heat islands and their relationship with impervious surface and vegetation abundance by using ASTER images. *Ieee Transactions on Geoscience and Remote Sensing*, *49*(10), 4080–4089.
Zhang, P., Imhoff, M. L., Wolfe, R. E., & Bounoua, L. (2010). Characterizing urban heat islands of global settlements using MODIS and nighttime lights products. *Canadian Journal of Remote Sensing*, *36*(3), 185–196.